

# Design and Experimental Study of a Probe for Crankshaft Full-automatic Measuring Machine

Meng-ting Xu, Hong-xi Wang\*, Ya-xiao Wang, Hui-hui Tian

*School of Mechatronic Engineering, Xi'an Technological University, 710021, Xi'an, China, wanghongxi@xatu.edu.cn*

**Abstract:** The Crankshaft Full-automatic Measuring Machine (CFMM) features high accuracy, high efficiency and complete measurement parameters, and represents the forefront of a geometric crankshaft accuracy measuring instrument. One of its core technologies is the high-precision radial following the crankshaft connecting rod journal measurement. In this paper, an independent probe design scheme combining the flexible dual-complex parallel four-bar guide mechanism and double displacement sensors based on the contact measurement method was proposed. It was suitable for the measurement of precision parts with eccentric characteristics such as crankshaft and camshaft measurement. Taking the spring as the flexible part, the probe prototype's optimization design, processing and assembly were completed, the test device was built, and the system accuracy was calibrated under various positions and feed quantities of the probe. The results revealed that the expanded measurement uncertainty after double-sensor compensation was enhanced from 1.53  $\mu\text{m}$  in single-sensor measurement to 0.44  $\mu\text{m}$ , satisfying the high-precision requirements of engineering measurement accuracy and reducing the measurement cost.

**Keywords:** Crankshaft, following measurement, flexible mechanism, probe.

## 1. INTRODUCTION

As one of the important parts of an engine, the crankshaft has various parameters that affect the overall quality of the engine. The crankshaft main journal diameter is about 50 mm and the connecting rod journal diameter is about 40 mm in a general automobile engine with a stroke of about 90 mm. To ensure its machining quality, precision inspection of this diameter is necessary. The Crankshaft Full-automatic Measuring Machine (CFMM) is the most advanced equipment for determining crankshaft machining accuracy. A key part of the comprehensive crankshaft measuring machine is the crankshaft probe, which is the core component used for radial measurements. The high-precision comprehensive crankshaft measuring machines produced by companies such as ADCOLE from the United States and HOMMEL and IBTL from Germany adopt their own proprietary follower measurement probe system, which is a complex and expensive non-independent system, and there are no commercial crankshaft probe products [1], [2]. Therefore, the research and development of general probe systems is essential to technically support the development of precision measurement equipment for eccentric rotating parts such as crankshafts and cams [3], [4].

Research on crankshaft measuring probes is still in the exploratory stage. For example, Geng Haixiang et al. combined an inductive displacement sensor and a grating

displacement sensor in their comprehensive camshaft measuring instrument [5]. The probe of this measuring instrument was a one-dimensional scanning probe, which required separate installation of the axial and radial probes, and was lacking in measurement accuracy. The full-automatic camshaft measuring instrument developed by Zhang Peiguo et al. used a vertical structure and a high-precision air-floating spindle, which achieved a unified reference [6]. However, the probe needed to be replaced frequently to meet the measurement requirements. Zhang Wei and Deng Yang adopted a plate-probe follow-up contact measurement for asymmetric shaft parts such as crankshafts and camshafts, and developed comprehensive measurement software for shaft parts based on the geometric error evaluation algorithm [7], [8]. The plane probe of this instrument exhibited a spindle rotation error, and the dynamic servo performance needed to be optimized for moving shafts. The automatic vehicle engine crankshaft detection system designed by Guo Hai integrates numerical control, data processing and computer technologies for precise crankshaft measurements [9]. However, the grating ruler of the experimental platform was not on the same axis as the measured crankshaft axis, resulting in the Abbé error.

Eccentric rotating parts are mostly measured by the active or passive following measurement method in which the main difficulty lies in the radial accuracy measurement of the eccentric part [10]. This paper analyzed the basic principles

for radial accuracy measurement of crankshaft connecting rod journals and the two basic forms of the following measurement system. A special probe for the CFMM based on the flexible guide rail was designed for the servo-following measurement system. To compensate for the Abbé error, detection with double sensors was used for the probe. The experimental results revealed that the expanded uncertainty of the radial measurement for the crankshaft probe could reach 0.44 μm.

2. DESIGN OF THE CRANKSHAFT MEASURING PROBE

A. Principle of crankshaft radial accuracy measurement

The principle of radial accuracy measurement of the crankshaft connecting rod journal is shown in Fig. 1. The coordinate origin *o* represents the rotation center of the crankshaft, *R* denotes the crankshaft stroke, *r* is the nominal radius of the connecting rod journal, and  $\delta$  represents the radius error of the connecting rod journal. When the crankshaft rotates by  $\varphi$ , the displacement in the *x*-direction of the radial measuring device is

$$x = R \cos \varphi + r + \delta$$

The displacement in the *x*-direction of the measuring device can be measured by the displacement sensor, so the radial dimension error of the connecting rod journal can be obtained as

$$\delta = x - R \cos \varphi - r$$

When the crankshaft rotates, the error at any point in the axial direction of the connecting rod journal can be obtained as

$$\delta_i = x_i - R \cos(\varphi_i) - r \tag{1}$$

where  $\varphi_i$  is given by the angular displacement sensor of the precision turntable.

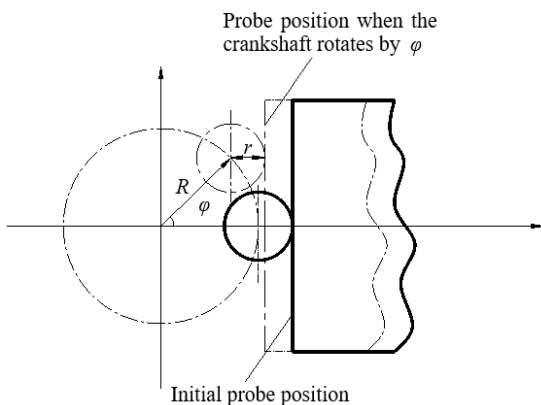


Fig. 1. Schematic diagram of radial measurement for the connecting rod journal.

The front measuring blade of the radial measuring system must remain in contact with the end face of the connecting rod journal during the measurements; i.e., the radial

measuring system must follow the movement of the connecting rod journal. This can be realized by passive following (follow-up) or active following (servo).

Follow-up mode

As shown in Fig. 2, the follow-up measurement system uses springs or gravity to enable constant contact between the measuring blade and the connecting rod journal, thereby maintaining a certain measuring force. The connecting rod journal rotates and drives the measuring blade and the motion table. The radial displacement is detected by a sensor for which the measurement error can be obtained by (1).

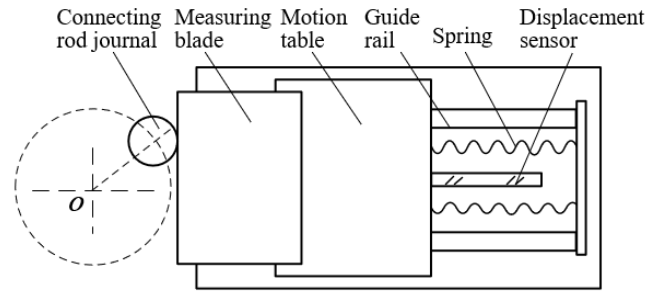


Fig. 2. Follow-up measurement scheme.

Servo mode

In servo mode, the measuring blade actively follows the position of the connecting rod journal, achieving reliable contact between the measuring head and the connecting rod journal. As shown in Fig. 3, the system uses the servo motor to drive the moving platform and moves according to the ideal positions of the connecting rod journal. However, due to the crankshaft processing error, the system cannot ensure good contact between the measuring rod and the connecting rod journal. Therefore, a special probe system that can detect linear movements within a small range and record displacements must be installed on the motion platform.

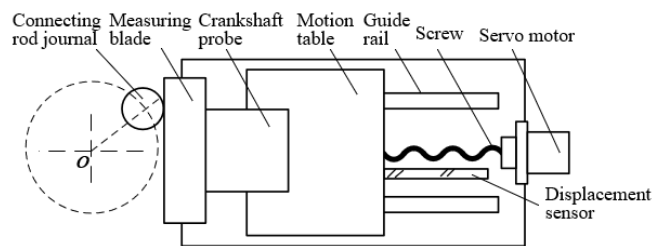


Fig. 3. Servo measurement scheme.

This paper focuses on the design, analysis and testing of the special probe in the servo radial crankshaft measurement system as shown in Fig. 3.

B. Probe system design

The scheme of the crankshaft probe is designed according to the servo measurement principle shown in Fig. 3. As shown in Fig. 4, the probe is mainly composed of a measuring blade in contact with the crankshaft, a guide rail capable of precise linear movements, a return spring that maintains a

certain contact force relative to the crankshaft, and a displacement sensor. To measure the radial error of the crankshaft connecting rod journal, the probe should have a certain pre-travel and the servo should follow the theoretical positions of the crankshaft.

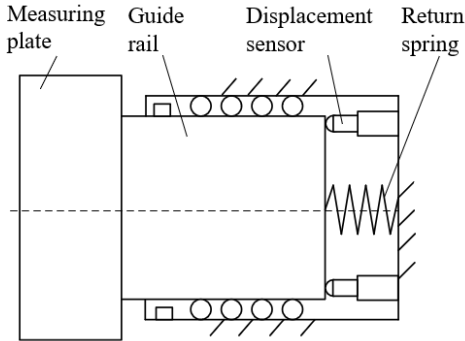


Fig. 4. Structural scheme of the crankshaft probe.

During the measurement process, due to the continuous change of the contact point between the crankshaft connecting rod journal and the measuring blade, the stress state of the guide rail is also changing, leading to a guiding error of the guide rail and thus to the Abbé error. Therefore, double displacement sensors are used to compensate for the Abbé error and improve the measurement accuracy [11]. The servo system itself has high tracking accuracy, so a motion

range of 1~2 mm is generally sufficient for the probe. The stiffness of the spring is designed according to the requirements of the contact force.

Commonly used motion guide mechanisms include the sliding guide rail, the rolling guide rail and the hydrostatic guide rail. For the crankshaft probe, which requires a range of 1~2 mm, flexible guide rail is used, which has no lubrication, a simple structure and no friction. The flexible guide rail is also a core mechanism of the scanning probe for numerically controlled measurement systems such as the coordinate measuring machine and gear measuring center.

C. Design of the flexible guiding mechanism

Selection of the flexible guiding mechanism

Common flexible guiding mechanisms include the parallel four-bar, double parallel four-bar and dual-complex parallel four-bar mechanisms [12], [13]. The dual-complex parallel four-bar mechanism shown in Fig. 5(c) is used in this design. Compared with those in Fig. 5(a) and Fig. 5(b), the mechanism in Fig. 5(c) has a larger measuring stroke and theoretically no coupling error. The flexure hinge uses the spring to eliminate the mechanical friction generated in the transmission process, since the spring exhibits small elastic deformation and rapid recovery [14], [15]. This choice improves the motion accuracy of the guide mechanism and avoids the need for lubrication.

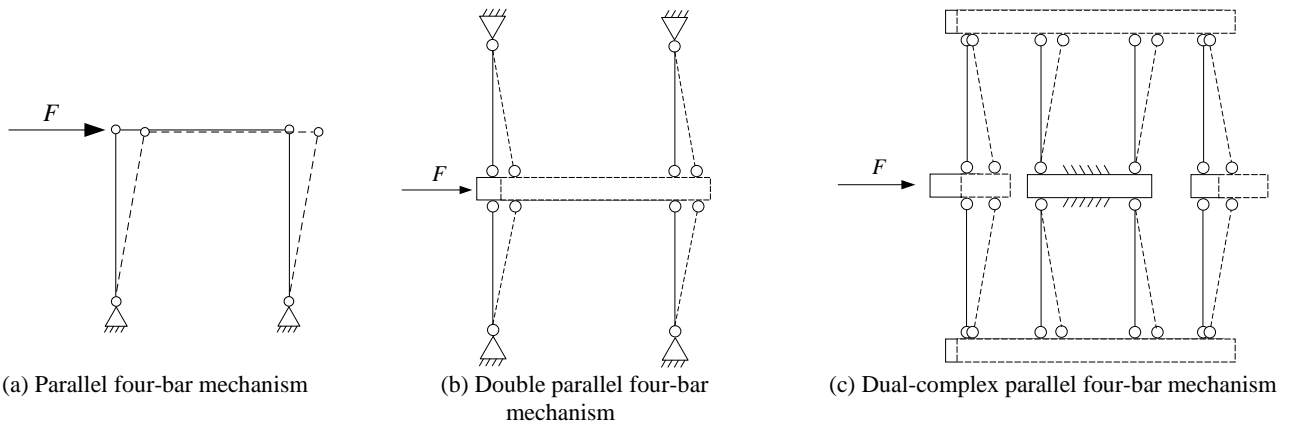


Fig. 5. Principles of common guiding mechanisms.

Parameter design and optimization of the flexible guiding mechanism

The commonly used flexure hinges have a structural form of semicircles or ellipses from direct integrated processing. The elastic spring is used as the elastic element in the assembly in this paper, as shown in Fig. 6(a), to improve fatigue resistance. Fig. 6(b) presents the assembly drawing of the flexible guide mechanism.

The stiffness in the moving direction of the guide mechanism is

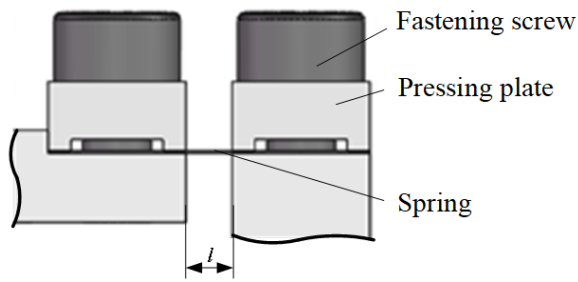
$$k_x = \frac{4Eb\theta^3}{3L\Delta^2x} = \frac{Eb\theta^3}{3L^2} \quad (2)$$

where  $E$ ,  $b$ ,  $l$  and  $h$  are the elastic modulus, width, length and

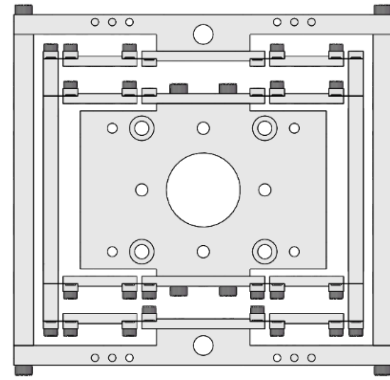
thickness of the spring, respectively, and  $L$  is the length of the connecting rod.

According to the requirements for the contact force between the measuring blade and the crankshaft, the parameters of the flexible guide mechanism were optimized according to (2). As shown in Fig. 7, when the spring thickness  $h$  was set to 0.1 mm, the spring length  $l$  was set to 2 mm, the spring width  $b$  was set to 50 mm, and the connecting rod length  $L$  was set to 25 mm, the stiffness in the moving direction was calculated to be 2.6 N/mm, meeting the measurement requirements.

The probe system displayed in Fig. 8 was designed according to the above parameters, and two GT21 pen inductive sensors were selected as the measuring elements.



(a) Flexure hinge connection



(b) Assembly drawing of the flexible guide mechanism

Fig. 6. Design of the dual-complex parallel four-bar mechanism.

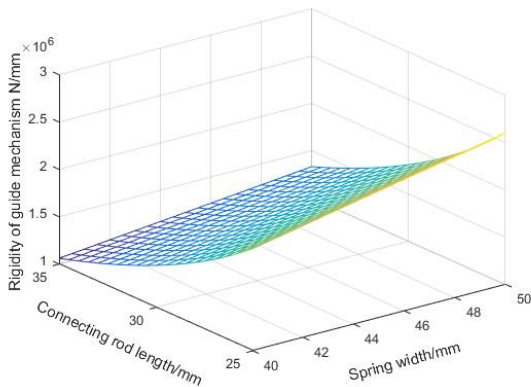


Fig. 7. Structural parameter optimization of the guide mechanism.

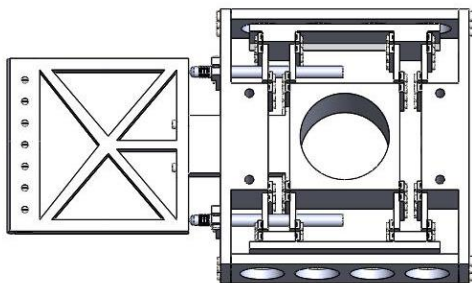


Fig. 8. Three-dimensional design for the probe of the crankshaft measuring machine.

### 3. EXPERIMENT ON MEASURING ACCURACY OF THE CRANKSHAFT PROBE

#### A. Experimental design

Attach the crankshaft probe and the digital display micrometer head (Sanfeng) to the base according to the experimental scheme shown in Fig. 9. During the measurement, rotate the feed of the micrometer head so the measuring blade retracts. The backward displacement of the measuring blade was output from sensor A and sensor B and read from the electronic display (TESA TT80). The farthest end of the measurement was on the center line of the two displacement sensors, and the distance between the two sensors was  $w$ . Measurements were taken at five equidistant points on the front end of the measuring rod. The feed

displacements of the micrometer head at each point were 0.2, 0.4, 0.6, and 0.8 mm, respectively. The readings from the two displacement sensors were recorded. Fig. 10 shows a photo of the measuring device.

According to the three-dimensional design drawing of the crankshaft measuring machine probe shown in Fig. 8 and the schematic diagram of the experimental scheme shown in Fig. 9, a measuring device consisting of two sensors, a compliant guiding mechanism, a measurement plate, a digital display micrometer head and an electronic length gauge was built, as shown in Fig. 10.

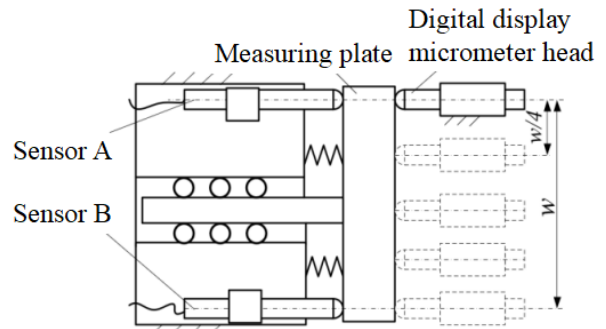


Fig. 9. Schematic diagram of the experimental scheme.

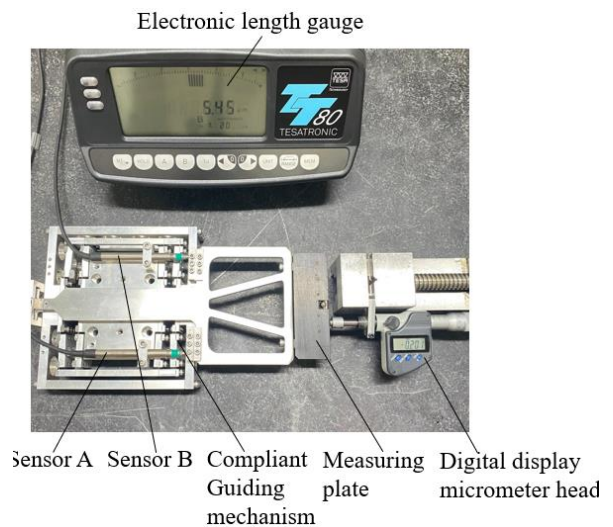


Fig. 10. Photo of the crankshaft probe device.

B. Processing and analysis of experimental results

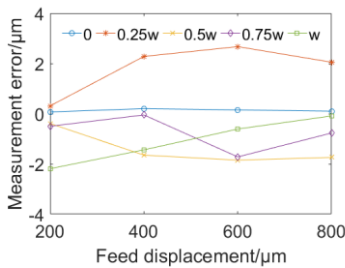
Error calculation

The experiments were conducted in three groups. The feed displacement of the micrometer head and the measured displacements of sensors A and B were recorded. The measured data are shown in Table 1. Theoretically, the

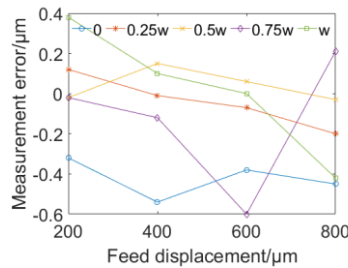
outputs of the two displacement sensors should be consistent. However, when the micrometer head set the measuring blade in motion, the readings from the two sensors inevitably deviated due to factors such as uneven forces and structural processing and assembly errors. Essentially, the geometric error of the movement of the flexible guide rail caused the Abbé error.

Table 1. Test data of the crankshaft probe.

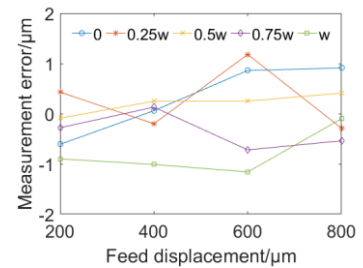
Experiment	Feed displacement / $\mu\text{m}$	Measuring position									
		0		0.25w		0.5w		0.75w		w	
		A	B	A	B	A	B	A	B	A	B
One	200	200.07	198.80	200.31	199.67	199.61	201.35	199.5	201.01	197.81	200.17
	400	400.20	400.30	402.28	398.46	398.35	400.68	399.95	401.80	398.56	400.26
	600	600.15	600.00	602.67	598.29	598.15	602.58	598.28	602.83	599.39	600.06
	800	800.10	799.30	802.05	798.45	798.26	801.97	799.23	802.86	799.91	800.08
Two	200	199.68	200.18	200.12	200.41	199.98	200.09	199.98	200.05	200.38	199.46
	400	399.46	400.26	399.99	399.94	400.15	400.24	399.88	400.34	400.10	399.37
	600	599.62	600.12	599.93	600.41	600.06	600.64	599.40	600.43	600.00	599.22
	800	799.55	800.16	799.80	800.61	799.97	800.55	800.21	800.63	799.58	799.97
Three	200	199.39	200.15	200.43	199.65	199.91	199.46	199.72	199.71	199.10	199.88
	400	400.06	399.75	399.80	400.09	400.25	399.28	400.13	400.56	398.99	399.78
	600	600.86	599.77	601.18	599.76	600.25	599.48	599.28	600.44	598.84	600.04
	800	800.91	799.75	799.71	800.36	800.41	798.90	799.46	799.84	799.90	800.40



(a) Experiment One

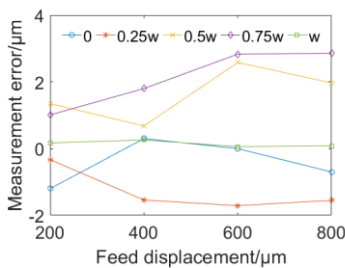


(b) Experiment Two

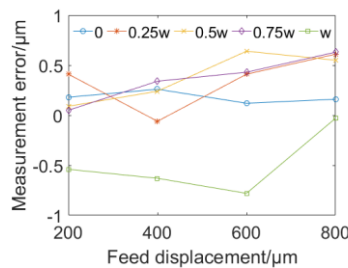


(c) Experiment Three

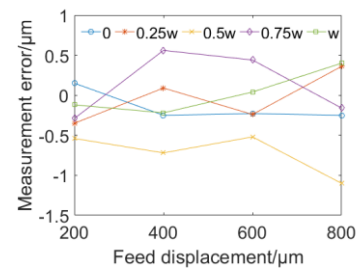
Fig. 11. Measurement error curves from sensor A.



(a) Experiment One



(b) Experiment Two



(c) Experiment Three

Fig. 12. Measurement error curves from sensor B.

Using the data in Table 1, the error curves were drawn when measuring with a single sensor, and the measurement errors of three groups of experiments were compared, as shown in Fig. 11 and Fig. 12.

The experimental results show that the roundness of the crankshaft connecting rod neck and the main journal requirements are generally 0.005 mm, when the accuracy of the probe should be less than 1 μm to meet the measurement requirements. As shown in Fig. 11 and Fig. 12, when a single displacement sensor was used in the probe system, measurement accuracy of less than 1 μm was difficult to achieve due to the Abbé error. To solve this problem, double displacement sensors were used to compensate for the error. According to the principle of linear interpolation, the actual displacement  $x$  of the probe can be obtained as

$$x = \frac{(x_B - x_A) \times y + x_A \times w}{w} \quad (3)$$

where  $y$  represents the position of the measuring contact point, and  $x_A$  and  $x_B$  denote the readings from sensors A and B, respectively. According to the double-sensor error compensation formula given by (3), the actual displacement of the probe was calculated at each measurement position, and the results are shown in Table 2.

The error curves from the double sensor measurement after error compensation were drawn according to the data in Table 2, and the comparison of the three groups of experiments is shown in Fig. 13.

As shown in Fig. 13, the experimental errors of the three dual-sensor groups were 0.48, 0.42, and 0.44 μm, respectively. Obviously, this method could effectively control the measurement error to within 0.5 μm after compensation and improve the measurement accuracy by 83% compared with the single-sensor measurement method.

Table 2. Actual displacements after error compensation in double-sensor measurement.

Experiment	Feed displacement /μm	Stress position				
		0	0.25w	0.5w	0.75w	w
One	200	200.07	199.83	200.12	199.98	200.17
	400	400.20	399.66	399.52	400.41	400.26
	600	600.15	599.63	600.32	599.90	600.06
	800	800.10	799.85	800.12	800.39	800.08
Two	200	200.18	200.34	200.04	200.00	200.38
	400	400.26	399.95	400.20	400.00	400.10
	600	600.12	600.29	600.35	599.66	600.00
	800	800.16	800.41	800.26	800.32	799.58
Three	200	200.15	199.85	199.69	199.72	199.88
	400	399.75	400.02	399.77	400.24	399.78
	600	599.77	600.12	599.87	599.57	600.04
	800	799.75	800.20	799.66	799.56	800.40

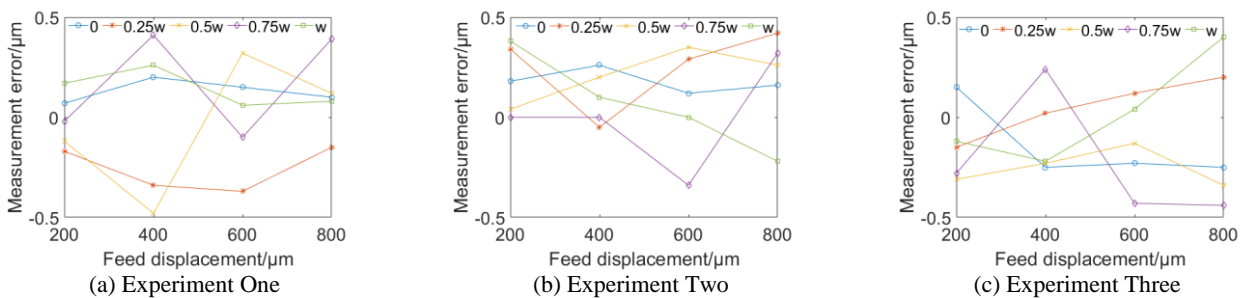


Fig. 13. Error curves after double-sensor error compensation.

*System uncertainty analysis*

The main factors that significantly influenced the uncertainty of the measurement results were the uncertainty  $u_a$  caused by measurement repeatability and the uncertainty  $u_b$  of the inductance measurement system. The measurement results were estimated according to the normal distribution to analyze the uncertainty of the measurement system [16].

*Uncertainty component  $u_a$  caused by measurement repeatability*

According to the Bessel formula, the standard deviation is calculated by

$$\sigma = \sqrt{\frac{\sum_{i=1}^n \vartheta_i^2}{n-1}} \quad (4)$$

The standard deviations of a single sensor,  $\sigma_{1A}$  or  $\sigma_{1B}$ , and the standard deviation of the double sensors  $\sigma_2$  were calculated separately, as shown in Table 3.

Table 3. Standard deviations of measurements.

Standard deviation $\sigma/\mu\text{m}$	Experiment One	Experiment Two	Experiment Three	Average
$\sigma_{1A}$	1.34	0.24	0.62	0.73
$\sigma_{1B}$	1.42	0.37	0.40	0.73
$\sigma_2$	0.24	0.16	0.23	0.21

The uncertainty components caused by measurement repeatability were  $u_{a1} = \sigma_1 = 0.73 \mu\text{m}$  and  $u_{a2} = \sigma_2 = 0.21 \mu\text{m}$ , with a degree of freedom of  $\nu_1 = \nu_2 = n-1 = 19$ .

*Uncertainty caused by indication error of the inductance measurement system  $u_b$*

According to the TT80 user manual, the measuring range of the micrometer is  $\pm 20 \mu\text{m}$ , and the indication error range is  $a = \pm 0.03 \mu\text{m}$ . Taking uniform distribution into account, the standard uncertainty is

$$u_b = \frac{a}{\sqrt{3}} \quad (5)$$

The standard uncertainty of micrometer indication was calculated to be  $u_b = 0.02 \mu\text{m}$  according to (5). Taking a relative standard deviation of  $\frac{\sigma_{u_3}}{u_3} = 25\%$ , the corresponding degree of freedom was  $\nu_3 = \frac{1}{2 \times 0.25^2} = 16$ .

*Combined uncertainty*

Since the uncertainty components  $u_a$  and  $u_b$  are independent of each other, the combined standard uncertainty is

$$u_c = \sqrt{u_a^2 + u_b^2} \quad (6)$$

The synthetic standard uncertainties were  $u_{c1} = 0.73 \mu\text{m}$  and  $u_{c2} = 0.21 \mu\text{m}$  according to (6), and the degree of freedom

of  $u_c$  was  $\nu_4 = \nu_5 = \frac{u_c^4}{\sum_{i=1}^N \frac{u_i^4}{\nu_i}} = 19$ .

*Expanded uncertainty*

Checking the  $t$ -distribution table for a confidence probability of  $P = 95\%$  and a degree of freedom of  $\nu = 19$  showed that  $t_{0.95}(19) = 2.09$ , i.e., the coverage factor  $k = 2.09$ . The expanded uncertainty  $U$  is

$$U = k u_c \quad (7)$$

According to (7), the expanded uncertainties of the single-sensor and double-sensor measurements were  $U_1 = 1.53 \mu\text{m}$ ,  $U_2 = 0.44 \mu\text{m}$ , respectively.

The results revealed significant Abbé error compensation of the double-sensor measurement method, which obviously improved the measurement accuracy compared with the single-sensor measurement method.

4. CONCLUSION

In this paper, a structural design and experimental scheme for a stand-alone probe component for the CFMM based on a flexible guide rail is proposed. The dual-complex parallel four-bar mechanism was used as the guiding mechanism, and the linear variable differential transformer was selected as the displacement measuring mechanism of the probe system to measure the error of any point in the axial direction of the connecting rod journal. The actual displacement of the probe was calculated by combining the error compensation formula with the simultaneous measurement of two sensors to eliminate the influence of the Abbé error on the experimental results and improve the measurement accuracy and repeatability. Within a measurement range of 1 mm, the expanded measurement uncertainty was reduced from 1.53  $\mu\text{m}$  to 0.44  $\mu\text{m}$  after double-sensor compensation. This shows a significant improvement in system accuracy and meets the precision measurement requirement for eccentric precision parts such as crankshafts and camshafts.

The dual-complex flexible mechanism used to guide the probe meant that there was no friction in the system. This indicated that there was no need for lubrication, which could meet the needs of eccentric shaft parts measuring equipment with servo control.

ACKNOWLEDGEMENTS

This work was funded by "Key Industrial Innovation Chain (Group) for Industry" Project of Shaanxi Provincial Science and Technology Department (2020ZDLGY14-02), and Industrialization Cultivation Project of Shaanxi Provincial Education Department (18JC014).

REFERENCES

[1] Zhang, Y., Yu, H., Pan, X. (2015). Geometrical error identification and compensation for grinding machine by crankshaft roundness measuring. *Chemical Engineering Transactions*, 46, 1099-104. <https://doi.org/10.3303/CET1546184>

- [2] Chybowski, L., Nozdrzykowski, K., Grządziel, Z., Jakubowski, A., Przetakiewicz, W. (2020). Method to increase the accuracy of large crankshaft geometry measurements using counterweights to minimize elastic deformations. *Applied Sciences*, 10 (14), 4722. <https://doi.org/10.3390/app10144722>
- [3] Fang, J., Hu, C., Pang, C., Liu, Y., Wang, L. (2015). Development and application of precision coordinate measuring technology. *Aeronautical Manufacturing Technology*, 7, 38-41.
- [4] Bosch, J.A. (2011). *Coordinate Measuring Machines and Systems*. New York: Marcel Dekker, Inc.
- [5] Geng, H. (2006). *Development of Fully Automatic Camshaft Flexible Measuring Instrument*. Sichuan: Sichuan University.
- [6] Zhang, P. (2010). *Research on Automatic Camshaft Measuring Instrument*. Xi'an: Xi'an Shiyou University.
- [7] Zhang, W. (2015). *Research on key Technology of Crankshaft and Camshaft Measuring Instrument*. Shanghai: Shanghai University.
- [8] Deng, Y. (2017). *Research on Key Technology of Automatic Comprehensive Measurement of Asymmetric Axis Parts*. Shanghai: Shanghai University.
- [9] Guo, H. (2017). *Design and Research of Vehicle Engine Crankshaft Automatic Detection System*. Xi'an: Xi'an University of Technology.
- [10] Yousuf, L.S., Marghitu, D.B. (2016). Experimental and simulation of a cam and translated roller follower over a range of speeds. In *International Mechanical Engineering Congress and Exposition*. ASME. <https://doi.org/10.1115/IMECE2016-65506>
- [11] Xie, C., Yuan, D., Ren, D., Zhao, H., Tao, X., Zhu, X. (2018). Calibration and compensation of dynamic abbe errors of a coordinate measuring machine. *Journal of Dynamic Systems, Measurement, and Control*, 140 (5), 051001. <https://doi.org/10.1115/1.4038171>
- [12] Yu, J., Pei, X., Bi, S., Zong, G., Zhang, X. (2010). Research progress on design method of flexure hinge mechanism. *Journal of Mechanical Engineering*, 46 (13), 2-13.
- [13] Awtar, S., Mariappan, D.D. (2017). Experimental measurement of the bearing characteristics of straight-line flexure mechanisms. *Precision Engineering*, 49, 1-14. <https://doi.org/10.1016/j.precisioneng.2016.12.014>
- [14] Zhao, Y., Liu, J., Han, L. (2007). Research on double compound parallel four-bar mechanism. *Aviation Precision Manufacturing Technology*, 4, 17-21.
- [15] Wang, H., Wang, Y., Bai, Z. (2012). Stiffness analysis and experimental test of planar flexure hinge steering mechanism. *Journal of Xi 'an Polytechnic University*, 32 (8), 631-635.
- [16] Papananias, M., Fletcher, S., Longstaff, A.P., Forbes, A.B. (2017). Uncertainty evaluation associated with versatile automated gauging influenced by process variations through design of experiments approach. *Precision Engineering*, 49, 440-455. <https://doi.org/10.1016/j.precisioneng.2017.04.007>

Received July 08, 2022

Accepted February 28, 2023